ELSEVIER

Chemical Physics 254 (2000) 349–361

Chemical Physics

www.elsevier.nl/locate/chemphys

Determination of the structures and barriers to hindered internal rotation of the phenol–methanol cluster in the S_0 and S_1 states

M. Schmitt *, J. Küpper, D. Spangenberg, A. Westphal

Heinrich-Heine-Universität Düsseldorf, Universitätsstraße 26.43.02, 40225 Düsseldorf, Germany

Received 13 December 1999

Abstract

The rotationally resolved $S_1 \leftarrow S_0$ electronic spectrum of the hydrogen-bonded phenol–methanol cluster has been analyzed. Due to the internal rotation of the methyl group in the methanol moiety, the spectrum of the electronic origin of phenol–methanol is split into A and E subtorsional bands. From a perturbation analysis of the torsional–rotational structure of the electronic origin, the threefold barriers to internal rotation of the methyl group could be determined to be 170 cm^{-1} in the S_0 state and 150 cm^{-1} in the S_1 state. The perturbation analysis yielded the angle between the internal rotor axis and the inertial axes of the cluster, which allows the determination of the geometry of the hydrogen bond in both electronic states.

1. Introduction

Binary hydrogen-bonded clusters of phenol with different solvent molecules such as water [1–13], methanol [1,14–18], ethanol [1,14,19,20], ammonia [21–27] have been investigated thoroughly, both experimentally and theoretically, as model systems for solvation processes of polar aromatic molecules. The acidity of phenol, like that of the other hydroxyaromates increases upon electronic excitation from the electronic ground state S_0 into the S_1 state. This increases the hydrogen bond strength in clusters in which phenol acts as the proton donor.

The fluorescence excitation spectrum of the phenol–methanol cluster, which is red shifted to the phenol monomer by 416 cm^{-1}, had first been published by Abe et al. [1]. They observed a vibronic band at 27 cm^{-1} which they assigned to a bending vibration that was not further specified and a band at 175 cm^{-1} which was assigned to the intermolecular stretching vibration. Using dispersed fluorescence spectroscopy, the frequencies of these vibrations could be determined in the electronic ground state to be 22 and 162 cm^{-1}, respectively [14]. The ionization potential of phenol$(CH_3OH)_1$ was determined via two color multiphoton ionization by Ito and coworkers for the first time [28]. They reported a value of 63 350 cm^{-1}, which was not corrected for the extraction field. A substantially more accurate value of 63 204 cm^{-1} was obtained by Wright et al. using zero kinetic energy electron (ZEKE) spectroscopy [15]. Hartland et al. performed ionization-loss stimulated Raman spectroscopy (ILSRS) on different hydrogen-bonded clusters, including the

* Corresponding author. Tel.: +211-81-13681; fax: +211-81-15195.

E-mail address: mschmitt@uni-duesseldorf.de (M. Schmitt).

0301-0104/00/$ - see front matter
PII: S0301-0104(00)00048-3

phenol–methanol cluster in the region of the intramolecular C–C and C–O stretching vibration [29]. To exclude that another conformer of phenol$(CH_3OH)_1$ absorbs in the observed spectral region, hole burning spectroscopy has been performed [17]. Moreover, the intermolecular vibrations, both in the S_0 and S_1-states, were assigned. More recently, a Fourier transform microwave spectrum of the phenol–methanol cluster has been taken by Stahl and coworkers [30,31], yielding rotational and centrifugal constants for the electronic ground state.

A theoretical analysis of the vibrations of the electronic ground state has been published by Gerhards et al. [16]. The predicted geometry on the Hartree–Fock level is translinear, as in the case of the phenol–water cluster. A more recent publication by Courty et al. presents a different structure of the cluster, based on a semi-empirical model potential, but unfortunately, no rotational constants for a direct comparison with our experimental results are reported [18]. In their proposed structure, the methyl group of the methanol moiety is bent considerably towards the aromatic ring, and the oxygen atom of the methanol moiety is slightly shifted off the phenol plane, which leads to a nonlinearity of the hydrogen bond.

The determination of the structural parameters of hydrogen-bonded clusters is a crucial and direct check for the quality of geometry predictions from high level theory. Rotationally resolved laser-induced fluorescence enables the determination of rotational constants in the electronic ground and excited states. Geometric changes upon electronic excitation which are due to changes in the electronic structure can, therefore, be investigated. Nevertheless, the knowledge of just three rotational constants for each electronic state allows at best the determination of three geometrical parameters such as bond lengths or angles. To evade this restriction, one can use isotopically substituted species of the investigated cluster and determine a substitution structure using Kraitchman's equations [32]. This is tedious, and in the case of larger molecules or clusters, a frequently impossible task.

The most important geometric parameters in hydrogen-bonded binary clusters are those which determine the orientation of the monomer moieties relative to each other. If only the relative orientation of the monomer units is of interest, six geometric parameters have to be determined. This, of course, is a rough approximation, as the structures of the monomers are also influenced by the cluster formation.

In the case of favorable symmetry of the cluster, the number of intermolecular parameters which have to be detected can sometimes be further reduced, and the determination of three rotational constants is sufficient for a description of the geometry of the hydrogen bond. This has been shown for the phenol$(H_2O)_1$ cluster, in which the plane containing the phenol molecule bisects the plane of the water moiety [6].

In the case of phenol$(CH_3OH)_1$, there are no symmetry constraints and all the intermolecular parameters are needed to describe the structure of the hydrogen bond. In this paper, we will show how the missing pieces of information for the determination of the geometry of the hydrogen bond in phenol$(CH_3OH)_1$ can be obtained from an analysis of the perturbation of the electronic spectrum by the hindered internal rotation of the methyl group. In a subsequent publication, we will compare these experimental results to the results of ab initio calculations.

2. Experimental setup

The experimental setup for the rotationally resolved laser induced fluorescence is described in detail elsewhere [33]. Briefly, the molecular beam machine consists of a triply differentially pumped vacuum apparatus. The expansion chamber is evacuated by a 8000 l/s oil diffusion pump (Leybold DI 8000), which is backed by a 250 m^3/h roots blower pump (Saskia RPS 250) and a 65 m^3/h rotary pump (Leybold D65B). In this way, a pressure below 1×10^{-4} mbar can be maintained in the expansion chamber up to a backing pressure of 3 bar of Ar, expanded through a 150 μm nozzle. The first skimmer, with an aperture of 1 mm, is located 10–25 mm downstream the nozzle orifice. The second chamber serves as a buffer chamber and is evacuated by a 360 l/s

turbomolecular pump (Leybold Turbovac 361), backed by a rotary pump (Leybold D16B), maintaining a pressure below 1×10^{-5} mbar. A second skimmer with an aperture of 2 or 3 mm, through which the collimated molecular beam enters the third chamber, is located at a variable distance of 120–190 mm downstream of the nozzle. This chamber is pumped by a 150 l/s turbomolecular pump (Leybold Turbovac 151) through a liquid nitrogen trap and backed by a rotary pump (Leybold D4B) resulting in a vacuum better than 1×10^{-6} mbar. The molecular beam is crossed at right angles with the laser beam at a distance of 360 mm downstream the nozzle. The resulting fluorescence is collected perpendicular to the two beams by an imaging optic consisting of a concave mirror and two lenses. The second lens focuses the fluorescence onto an iris aperture for further spatial filtering of the emitted fluorescence.

The laser system consists of a commercially available ring dye laser (Coherent 899-21) which is pumped with 6 W of the 514 nm line of an Ar^+-ion laser (Coherent Innova 100). Operated with Rhodamine 110 and Rhodamine 6G dyes, output powers of typically 0.5–1 W with a single mode line width of approximately 600 kHz can be obtained. This light is coupled into an externally folded ring cavity (LAS WaveTrain) for second harmonic generation (SHG). In order to ensure a high incoupling efficiency to the doubling cavity, the incoming laser beam is mode matched with the cavity mode by means of a projection lens. The cavity length is actively stabilized to enhance the frequency conversion of the single mode laser by a piezo-mounted mirror, driven by the error signal of a Coulliaud–Hänsch type stabilization unit [34]. With resonance enhancements in the cavity of approximately 50–80, a UV output power of 10–20 mW can be achieved.

The absolute frequency of the dye laser is determined by comparison of the transitions in an iodine absorption spectrum taken simultaneously with the LIF spectrum, to the tabulated iodine transition frequencies from Ref. [35]. The relative frequencies were determined by a mode matched confocal Fabry–Perot interferometer with a free spectral range of 149.9434(56) MHz.

3. Theory

The point group of the phenol–methanol cluster is C_1. The internal rotation of the methyl group can be described by a cyclic permutation of the hydrogen atoms, resulting in the molecular symmetry group G_3. This group consists of the identity operation E and the permutations (123) and (132) [36].

The overall wave function must have even parity for both the permutations and therefore transforms like A.

$$\begin{aligned}\Gamma(\Psi_{\text{tot}}) = \Gamma(\Psi_{\text{el}}) \otimes \Gamma(\Psi_{\text{vib}}) \otimes \Gamma(\Psi_{\text{tor}}) \\ \otimes \Gamma(\Psi_{\text{rot}}) \otimes \Gamma(\Psi_{\text{ns}}) \supseteq A.\end{aligned} \tag{1}$$

The electronic and vibrational wave functions Ψ_{el} and Ψ_{vib} transform like A because under supersonic jet conditions, only the vibronic ground state is populated. The transformation properties of the torsional wave functions Ψ_{tor} can be deduced from the correlation of the transformation properties of the harmonic oscillator and free rotor limiting cases. The torsional wave function of lower energy transforms like A, the energetically following like E. They can be expanded in the basis of free rotor functions as

$$\Psi_{\text{tor}} = |v, \sigma\rangle = \sum_{k=-\infty}^{\infty} A_{3k+\sigma}^{(v)} e^{i(3k+\sigma)\alpha}, \tag{2}$$

where v is the torsional state index and the integer σ can take the values 0 and ± 1 for A and E levels, respectively. The selection rule for the torsional transitions is $\Delta\sigma = 0$, because the transition dipole moment is independent of the torsional angle α for the symmetric rotor $-CH_3$, which leads to $A \leftrightarrow A$ and $E \leftrightarrow E$ torsional transitions.

The rotational wave functions Ψ_{rot} transform like A, irrespective of the parity of K_a and K_c. The spin wave functions Ψ_{ns} transform like $4A + 2E$. Because the overall wave function transforms like A, the spin statistical weight between the $\sigma = 0$ (A) and $\sigma = 1$ (E) subbands is 1:1.

The coupling between the internal rotation of the methyl group and the overall rotation of the cluster is treated in the formalism of the principal axis method (PAM) [37,38]. The Hamiltonian for

a molecule undergoing internal and overall rotation is

$$\widehat{H} = \widehat{H}_{\mathrm{R}}^{(A)} + \widehat{H}_{\mathrm{T}} + \widehat{H}_{\mathrm{RT}}, \tag{3}$$

where $\widehat{H}_{\mathrm{R}}^{(A)}$ is the Hamiltonian for a distortable rotor in Watson's A-reduced form [39,40]

$$\begin{aligned}\widehat{H}_{\mathrm{R}}^{(A)} = {} & B_x^{(A)}P_x^2 + B_y^{(A)}P_y^2 + B_z^{(A)}P_z^2 - \Delta_J P^4 \\ & - \Delta_{JK}P^2P_z^2 - \Delta_K P_z^4 - 2\delta_J P^2\left(P_x^2 - P_y^2\right) \\ & - \delta_K\left[P_z^2\left(P_x^2 - P_y^2\right) + \left(P_x^2 - P_y^2\right)P_z^2\right]\end{aligned} \tag{4}$$

and H_{T} is the torsional Hamiltonian

$$\widehat{H}_{\mathrm{T}} = Fp^2 + \sum_{n=1}^{6} V_n(1 - \cos n\alpha), \tag{5}$$

which depends only on the torsional angle α and can therefore be treated separately. F is the torsional constant and defined by

$$F = \frac{h}{8\pi^2 r I_\alpha} \tag{6}$$

with

$$r = 1 - \sum_{g=a,b,c} \frac{\lambda_g^2 I_\alpha}{I_g}, \tag{7}$$

where λ_g are the direction cosines between the inertial axes and the axis of internal rotation, I_α the moment of inertia of the internal rotor with respect to its symmetry axis and, I_g the principal moments of inertia of the whole molecule. The molecule fixed axes a, b, c are identified with the space fixed axes of Eq. (4) using the representation I^r. The rotational constants $B_x^{(A)}, B_y^{(A)}$ and $B_z^{(A)}$ in Eq. (4) have to be corrected for the contribution of the centrifugal distortion [40] thus yielding the geometrical rotational constants A, B and C. The coupling between the internal and overall rotation is described by the third term $\widehat{H}_{\mathrm{RT}}$ in Eq. (3). In the high barrier limit, this coupling term is small and can be evaluated by the perturbation theory. In principle, the harmonic oscillator wave functions are a more adequate basis set in the high barrier limit. Using a large enough basis set of free rotor wave functions is an equivalent *ansatz*. The torsion–rotation coupling has been treated by second-order perturbation theory. It yields the torsion–rotation Hamiltonian [37,41]

$$\begin{aligned}\widehat{H}_{\mathrm{RT}} = {} & FW_{v\sigma}^{(1)}(\rho_a P_a + \rho_b P_b + \rho_c P_c) \\ & + FW_{v\sigma}^{(2)}(\rho_a P_a + \rho_b P_b + \rho_c P_c)^2.\end{aligned} \tag{8}$$

The first-order perturbation coefficients $W_{v\sigma}^{(1)}$ are zero for A levels, while $W_{v\sigma}^{(2)}$ is nonzero for both A and E levels. The coefficients ρ_g with $g = a, b, c$ are defined as

$$\rho_g = \lambda_g \frac{I_\alpha}{I_g}. \tag{9}$$

The nth order perturbation coefficients $W_{v\sigma}^{(n)}$ are defined by [37]

$$W_{v\sigma}^{(0)} = \frac{E_{v\sigma}}{F}, \tag{10}$$

$$W_{v\sigma}^{(1)} = -2\langle v, \sigma|p|v, \sigma\rangle, \tag{11}$$

$$W_{v\sigma}^{(2)} = 1 + 4F\sum_{v'} \frac{|\langle v, \sigma|p|v', \sigma\rangle|^2}{E_{v\sigma} - E_{v'\sigma}}, \tag{12}$$

where $|v, \sigma\rangle$ are eigenfunctions of Eq. (5) and $E_{v\sigma}$ are the respective eigenvalues with v as the torsional state index and σ as defined above. The zero-order perturbation coefficients represent the solutions of Eq. (5) and will be needed in the sequel. The second term of Eq. (8) gives rise to cross terms in the angular momenta of the kind $\rho_g\rho_{g'}P_gP_{g'}$ with $g \neq g'$. If they are small enough to be neglected, the second-order perturbation terms are quadratic in the angular momenta with respect to the inertial axes and can therefore be incorporated in the rotational Hamiltonian (4) with effective rotational constants defined by

$$A_{v\sigma} = A + FW_{v\sigma}^{(2)}\rho_a^2, \tag{13}$$

$$B_{v\sigma} = B + FW_{v\sigma}^{(2)}\rho_b^2, \tag{14}$$

$$C_{v\sigma} = C + FW_{v\sigma}^{(2)}\rho_c^2. \tag{15}$$

Thus, the A subband can be fitted to Watson's A-reduced Hamiltonian with three effective rotational constants $A_{v\sigma}, B_{v\sigma}$ and $C_{v\sigma}$ and five centrifugal distortion constants $\Delta_J, \Delta_{JK}, \Delta_K, \delta_J$ and δ_K for each electronic state, while the E torsional subband is fitted to 11 parameters for each electronic state, namely three effective rotational constants,

the five centrifugal distortion constants and the three torsion–rotation constants D_a, D_b and D_c

$$\begin{aligned}\widehat{H}_{v\sigma} &= A_{v\sigma}P_a^2 + B_{v\sigma}P_b^2 + C_{v\sigma}P_c^2 \\ &\quad + \Delta_J P^4 - \Delta_{JK}P^2P_a^2 - \Delta_K P_a^4 - 2\delta_J P^2\left(P_b^2 - P_c^2\right) \\ &\quad - \delta_K\left[P_a^2\left(P_b^2 - P_c^2\right) + \left(P_b^2 - P_c^2\right)P_a^2\right] \\ &\quad + D_aP_a + D_bP_b + D_cP_c \qquad (16)\end{aligned}$$

with

$$D_g = FW_{v1}^{(1)}\rho_g. \qquad (17)$$

Generally, the barrier to internal rotation can be obtained from these D coefficients, or from the difference of the effective rotational constants for the A and E lines, which yields the difference of the second-order perturbation coefficients:

$$\Delta A = A_{v0} - A_{v1} = F\rho_a^2\left[W_{v0}^{(2)} - W_{v1}^{(2)}\right], \text{ etc.} \qquad (18)$$

Due to the smallness of $\Delta A, \Delta B$ and ΔC and the inherently large errors in determining the differences of large numbers, we tread only the first path for the determination of the barriers to internal rotation in the following.

4. Results and discussion

From a UV–UV double resonance spectrum, it could be concluded that, in the region of the intermolecular vibrations of phenol–methanol, only one conformer gives rise to absorptions [17]. Fig. 1 shows a part of the rotationally resolved LIF spectrum of the electronic origin of the phenol$(CH_3OH)_1$ cluster. The electronic origin of phenol–methanol is split into two subbands due to the internal rotation of the methyl group in the methanol moiety. The origins of the A ↔ A and E ↔ E subbands which are marked by arrows in Fig. 1 are 3557.621 MHz apart. The origin of the E subband is shifted to the blue region, indicating a lowering of the torsional barrier in the S_1 state. 261 transitions of the A subband with an assumed uncertainty for each line of 4 MHz were fitted to Watson's A-reduced Hamiltonian (Eq. (4)) in the representation I^r, yielding the effective rotational constants (Eqs. (13)–(15)) and centrifugal distortion coefficients for both the electronic states, which are given in Table 1.

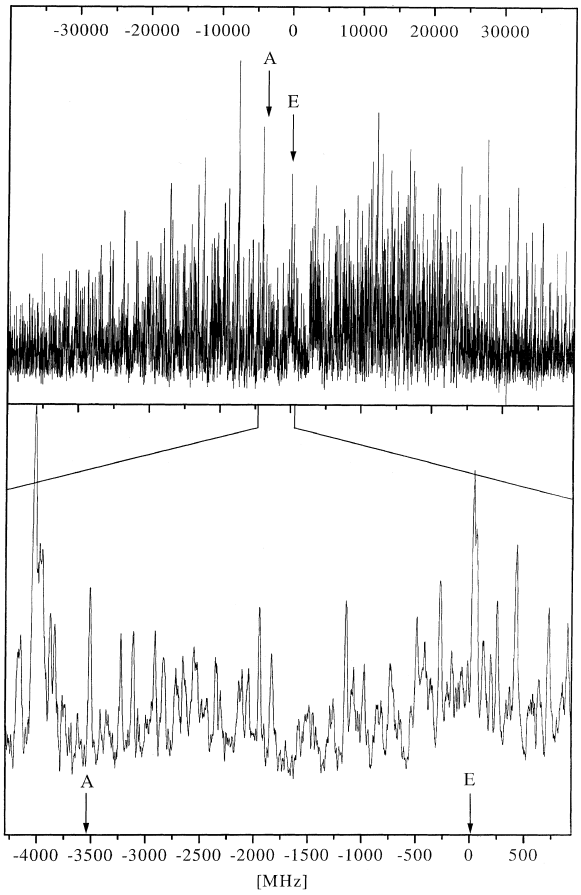

Fig. 1. Rotationally resolved LIF spectrum of the electronic origin of phenol$(CH_3OH)_1$. The origins of the A and E subbands are marked by arrows. The lower trace shows an enlarged portion of the spectrum in the region of the electronic origin of both subbands.

193 lines of the E ↔ E subband with an assumed uncertainty for each line of 4 MHz have been fitted to the torsion–rotation Hamiltonian (16). The effective rotational constants, centrifugal distortion and torsion–rotation constants for both the electronic states are given in Table 1. Fig. 2 shows a part of the electronic origin of phenol$(CH_3OH)_1$ together with a fit of the A and E torsional subspectrum.

The overall shape of the electronic origin could be simulated with an *a*/*b*/*c* hybrid ratio of 26:70:4 and a rotational temperature of 5 K.

Table 1
Effective rotational constants, centrifugal distortion and torsion–rotation constants for the A and E subband of phenol$(CH_3OH)_1$ in the ground and electronically excited state[a]

	S_0		S_1	
	A	E	A	E
$A_{v\sigma}$ (MHz)	3290.955(117)	3290.723(212)	3311.333(105)	3310.151(155)
$B_{v\sigma}$ (MHz)	792.126(80)	792.2965(901)	775.896(73)	775.8760(868)
$C_{v\sigma}$ (MHz)	685.8108(657)	685.4643(633)	664.3170(661)	664.2267(619)
Δ_J (kHz)	0.313(246)	0.963(240)	0.207(228)	0.113(268)
Δ_{JK} (kHz)	−5.17(113)	−5.51(245)	−3.82(108)	−0.17(18)
Δ_K (kHz)	23.92(210)	18.26(503)	12.91(181)	5.57(306)
δ_J (kHz)	0.002(145)	0.1106(1343)	0.096(132)	−0.0652(1397)
δ_{JK} (kHz)	−17.2(144)	41.2(150)	−5.0(138)	−5.0(114)
D_a (MHz)	–	32.83(34)	–	78.90(32)
D_b (MHz)	–	14.3(78)	–	38.2(34)
D_c (MHz)	–	40.312(183)	–	52.134(187)
v_0 (cm^{-1})	–	–	35932.85(2)	35932.97(2)
$v_0(E) - v_0(A) = 3557.621(740)$ MHz	–	–	–	–

[a] The number of digits retained for each parameter were calculated according to the scheme of Watson [48] , so that the calculated standard deviation of the fit can be reproduced within 10%.

Due to the comparably high temperature of 5 K, the small subtorsional splitting of approximately 0.1 cm^{-1} and the small rotational constants, the LIF spectrum is relatively congested. Only few lines could be identified as single rovibronic transitions and used for a line shape fit to a Voigt profile. Therefore, there is a large uncertainty in the determination of the Lorentzian contribution. The best fit gave a Lorentzian line width of 20 ± 5 MHz with a Gaussian (Doppler) contribution of 9 MHz, resulting in a fluorescence lifetime of 7.9 ± 2.5 ns.

4.1. Perturbation treatment of the internal rotation

From the experimentally determined rotational and rotational–torsional constants, the direction cosines λ_g between the internal rotor axis and the inertial axes of the cluster can be calculated. Eqs. (9) and (17) and the relation $\lambda_a^2 + \lambda_b^2 + \lambda_c^2 = 1$ yield

$$\lambda_a = \pm \frac{D_a I_a}{\sqrt{D_a^2 I_a^2 + D_b^2 I_b^2 + D_c^2 I_c^2}},$$
$$\lambda_b = \pm \frac{D_b I_b}{\sqrt{D_a^2 I_a^2 + D_b^2 I_b^2 + D_c^2 I_c^2}},$$
$$\lambda_c = \pm \frac{D_c I_c}{\sqrt{D_a^2 I_a^2 + D_b^2 I_b^2 + D_c^2 I_c^2}}, \qquad (19)$$

where each sign is undetermined, but all the signs for λ_a, λ_b and λ_c are equal. The direction cosines will be used in the determination of the geometrical structure of the cluster in Section 4.2. Plusquellic and Pratt showed the possibility of determining the signs of the D_gs from an intensity analysis [42]. In this work, however, we were not able to determine the signs of the D_gs due to the small absolute values of these constants, resulting in negligible intensity differences for changing the signs of the D_gs in one electronic state. The moments of inertia I_g to be used in Eq. (19) have been calculated from the effective rotational constants of the A and E subspectra, using the relation [41],

$$I_a = \frac{h}{8\pi^2\left(\frac{1}{3}A_{v0} + \frac{2}{3}A_{v1}\right)}, \text{ etc.} \qquad (20)$$

From the experimental constants also, the first-order perturbation coefficients $W_{v1}^{(1)}$ (Eq. (17)) can be determined:

$$W_{v1}^{(1)} = \frac{8\pi^2 r\sqrt{D_a^2 I_a^2 + D_b^2 I_b^2 + D_c^2 I_c^2}}{h} \qquad (21)$$

with r defined by Eq. (7). I_α, the moment of inertia of the methyl group was fixed to the value in free methanol (3.2122 amu Å^2).

Table 2 gives the values for the direction cosines between the internal rotor axis and the inertial

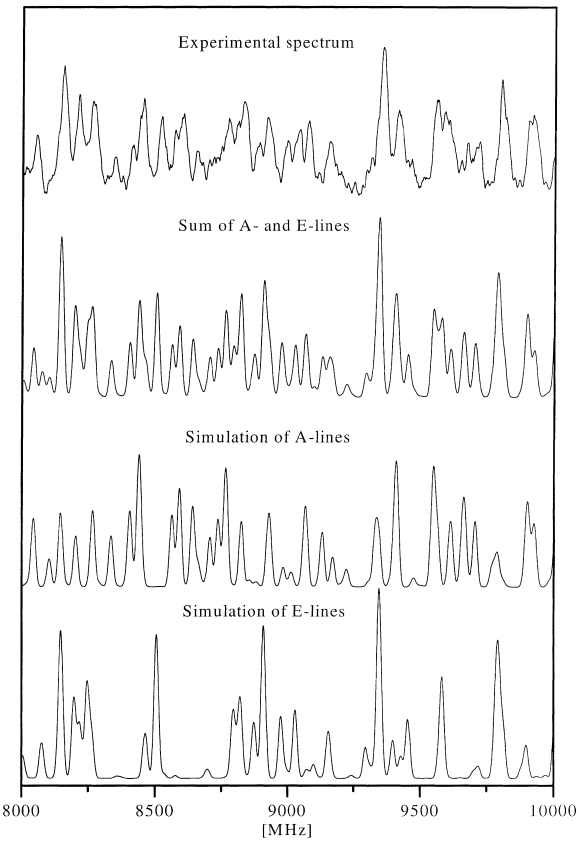

Fig. 2. Enlarged portion of the rotationally resolved LIF spectrum of phenol$(CH_3OH)_1$ (upper trace). The other traces show the simulations of the A and E subtorsional spectra and a superposition of both A and E lines for comparison with the experiment. The molecular constants used in the simulations are given in Table 1.

axes of the cluster and the respective angles of both electronic states. The internal rotor constant F is calculated using Eq. (6) to be 158.1 GHz (5.27 cm^{-1}) for the electronic ground state and 158.2 GHz (5.28 cm^{-1}) for the excited state.

From the first-order perturbation coefficients, the reduced barrier height V_n/F can be evaluated, using Herschbach's tabulated perturbation coefficients [41]. The reduced barrier height V_n/F of both the electronic states is given in Table 2. Using the above calculated results of 158.1 and 158.2 GHz for F, V_3-barriers of 5084.6 GHz (170 cm^{-1}) and 4374.5 GHz (146 cm^{-1}) for the S_0 and S_1 states, respectively, are obtained. From Herschbach's

Table 2
Direction cosines, angles between inertial axes and internal rotation axis, reduced barriers to internal rotation of the methyl group and geometrical rotational constants in the S_0 and S_1 states of phenol$(CH_3OH)_1$[a]

	S_0	S_1
λ_a	±0.1601(75)	±0.2492(60)
λ_b	±0.298(150)	±0.5144(340)
λ_c	±0.944(43)	±0.8205(195)
$\angle(a,i)$ (°)	80.78(44)/99.2	75.57(35)/104.4
$\angle(b,i)$ (°)	73.15(870)/106.9	59.04(230)/120.9
$\angle(c,i)$ (°)	19.34(750)/160.7	34.86(200)/145.1
V_3/F	32.16(49)	27.65(24)
F (MHz)	158094(4)	158192(4)
A (MHz)	3290.8(1)	3310.5(1)
B (MHz)	792.19(7)	775.89(6)
C (MHz)	685.62(5)	664.25(5)

[a] The second angle is $180 - \angle(g,i)$ for the reverse sign of λ_g. For a discussion of the internal rotor constant F, see the text.

tables also the zero-order perturbation coefficients $W_{v\sigma}^{(0)}$, which give the energy of the torsional sublevel divided by F, can be obtained for both the $\sigma = 0$ and $\sigma = 1$ states. From the difference $F''(W_{v1}^{(0)} - W_{v0}^{(0)})'' - F'(W_{v1}^{(0)} - W_{v0}^{(0)})'$, the A–E splitting of the electronic origin can be calculated to be 3995 ± 650 MHz. Comparison with the experimental value of 3557.621 MHz confirms the correctness of the above considerations.

The calculated V_3 barriers in both the electronic states are considerably lower than the barrier in free methanol, which was found to be 376.8 cm^{-1} [43]. This reduction in barrier height upon complexation had been observed before in the methanol dimer, where the barrier to internal rotation in the acceptor methanol was determined to be 120 cm^{-1} [44]. Fraser et al. [45] showed that this apparent reduction is an artifact due to the coupling between two internal motions, which are the internal rotations of the methyl group and the librational motion of the methanol molecule about its inertial a-axis. The stronger the methanol molecule is bound to the other cluster component, the larger is the hindrance potential for the librational motion and the closer is the F value to the contribution from the moment of inertia of the methyl top (5.26 cm^{-1}).

On the other hand, a weak bond implies an F which is closer to 27.6 cm^{-1}, the value in free

methanol, because the methanol molecule can undergo a large amplitude motion in the shallow intermolecular potential. The A–E splitting is a function of the reduced barrier height V_n/F. Thus, a small F value only pretends a low V_3 barrier. Instead of using the limiting value of F which was obtained by neglecting the coupling to the librational motion, we can also assume that the "true" barrier of the methanol moiety is not altered by complexation from the value of the monomer (376.8 cm^{-1}). Under this assumption, an F value of 12.1 cm^{-1} in the electronic ground state is obtained.

With the second-order perturbation coefficients, which have been obtained from Herschbach's tabulated perturbation coefficients [41], we could correct the rotational constants using Eqs. (13)–(15). The resulting geometrical rotational constants, which are used for the determination of the structure, performed in Section 4.2, are presented in Table 2.

4.2. Determination of the structure

The geometrical rotational constants and the angles between the inertial axes of the cluster and internal rotor axis given in Table 2 can now be used to determine the intermolecular geometry.

For each electronic state, we could determine three rotational constants A, B, C and additionally three (absolute values of the) angles between the internal rotor axis i and the inertial axes a, b and c of the cluster. However, one of these angles is redundant because it does not reduce the total number of four independent orientations of i which are given by the other two angles.

For the monomer moieties of the cluster, we assumed the same geometries as in the uncomplexed molecules. The complete substitution structure of phenol in the electronic ground state has been published by Larsen [46], the r_s structure of methanol is reported by Gerry et al. [43]. If we neglect the geometry changes of the monomer units upon cluster formation, 12 unknown parameters remain. These are the three coordinates, which describe the translation of the center of mass (COM_P^{PM}) of phenol within the principal axis system of the cluster ($x_{COM_P^{PM}}, y_{COM_P^{PM}}, z_{COM_P^{PM}}$), the three angles, which describe the rotation of the phenol moiety (θ_P, ϕ_P, χ_P), the three coordinates for the translation of the COM_M^{PM} of methanol (M) within the cluster system ($x_{COM_M^{PM}}, y_{COM_M^{PM}}, z_{COM_M^{PM}}$), and the three angles, describing the rotation of the methanol part (θ_M, ϕ_M, χ_M).

These 12 unknown parameters face 11 independent conditions. These are the six elements of the inertia tensor which is diagonal for the chosen reference system (the principal axis system of the cluster):

$$\begin{aligned} I_x &= \sum_i m_i(y_i^2 + z_i^2), \\ I_y &= \sum_i m_i(x_i^2 + z_i^2), \\ I_z &= \sum_i m_i(y_i^2 + x_i^2), \\ I_{xy} &= I_{yx} = -\sum_i m_i x_i y_i = 0, \\ I_{xz} &= I_{zx} = -\sum_i m_i x_i z_i = 0, \\ I_{zy} &= I_{yz} = -\sum_i m_i z_i y_i = 0. \end{aligned} \tag{22}$$

The moments of inertia are obtained from the rotational constants A, B and C of the cluster which have been determined experimentally. Furthermore, three conditions for the relative positions of COM_P^{PM} and COM_M^{PM}. Considering phenol and methanol as point masses M_P and M_M, respectively, we have

$$COM_M^{PM} = \begin{pmatrix} x_{COM_M^{PM}} \\ y_{COM_M^{PM}} \\ z_{COM_M^{PM}} \end{pmatrix} = -\frac{M_P}{M_M} \begin{pmatrix} x_{COM_P^{PM}} \\ y_{COM_P^{PM}} \\ z_{COM_P^{PM}} \end{pmatrix} \tag{23}$$

and finally two angles, describing the orientation of the internal rotor axis i with respect to the inertial axes of the cluster, which have been determined experimentally.

The transformation of the phenol monomer (P) coordinates $\vec{r}_i^{\,P}$ into the corresponding cluster (PM) coordinates $\vec{r}_i^{\,PM}$ can be expressed as

$$\vec{r}_i^{\,PM} = \mathbf{S}(\theta_P, \phi_P, \chi_P)\vec{r}_i^{\,P} - \begin{pmatrix} x_{COM_P^{PM}} \\ y_{COM_P^{PM}} \\ z_{COM_P^{PM}} \end{pmatrix}, \tag{24}$$

where θ_P, ϕ_P and χ_P are the Eulerian angles and $\mathbf{S}(\theta, \phi, \chi)$ is the direction cosine matrix [47, p. 80].

The orientation of the rotor axis does not completely determine the orientation of the methanol molecule. To obtain a unique solution, a simplification of the model has to be introduced. We consider the methanol molecule as a dumb-bell being composed of the point masses M_{OH} and M_{CH_3} of the hydroxyl and methyl groups, located at their respective centers of mass within the methanol frame, COM^{M}_{OH} and $COM^{M}_{CH_3}$. A close examination of the methanol structure as given by Gerry et al. [43] reveals that the internal rotor axis of the methyl top deviates less than 1° from the line connecting the COM of the methyl and hydroxyl group (COM_{CH_3}–COM_{OH}). In comparison, the angle between the rotor axis and the C–O bond is 3.2°. Therefore, we can treat the dumb-bell in good approximation as if the connection between the two point masses were identical to the internal rotor axis of methanol. This implies that its center of mass $COM_{CH_3,OH} \equiv COM_M$ lies on this axis. The distances of the COM of the hydroxyl group and the methyl group from the COMs of the cluster are given by

$$\vec{r}^{PM}_{OH} = COM^{PM}_{M} + \frac{M_{CH_3}}{M_{CH_3OH}} d(COM_{CH_3}\text{–}COM_{OH}) \begin{pmatrix} \pm\lambda_a \\ \pm\lambda_b \\ |\lambda_c| \end{pmatrix}, \tag{25}$$

$$\vec{r}^{PM}_{CH_3} = COM^{PM}_{M} + \frac{M_{OH}}{M_{CH_3OH}} d(COM_{CH_3}\text{–}COM_{OH}) \begin{pmatrix} \pm\lambda_a \\ \pm\lambda_b \\ |\lambda_c| \end{pmatrix}, \tag{26}$$

where COM^{PM}_{M} is determined from Eq. (23) and the distance $d(COM_{CH_3}\text{–}COM_{OH})$ has been calculated to be 1.517 Å from the r_s structure given in Ref. [43].

As already mentioned, even the orientation of the internal rotor axis is not unambiguously defined since we do not know the (absolute) signs of the direction cosines λ_g (cf. Eq. (19)). There are four distinguishable combinations of signs, hence we expect four different solutions. In our calculations, we positioned the COM of the methyl and hydroxyl groups according to each one of the four combinations of angles and the center of mass condition (23) and solved the six equations of the moment of inertia tensor (22) for the remaining parameters $x_{COM^{PM}_P}, y_{COM^{PM}_P}, z_{COM^{PM}_P}, \theta, \phi$ and χ numerically. Eq. (24) was used to determine the position of the phenol atoms in the coordinate system of the cluster and Eqs. (25) and (26) to determine the position of the COM of the methyl and hydroxyl groups in the coordinate system of the cluster.

These Cartesian coordinates were transformed to internal coordinates to compare our experimentally determined structure to the proposed theoretical structure from Ref. [18]. Table 3 and Fig. 3 gives the definitions of the internal coordinates in the S_0 state.

The structures are denoted by $1_0 \ldots 4_0$, the subscript refers to the S_0 state. The first line of Table 3 identifies the four possible orientations of the internal rotor axis. These four orientations are shown in Fig. 4a. From the given signs, we can conclude the relative signs of the rotational constants D_g. Table 3 also lists the angles between the transition dipole moment and the inertial axes of the cluster. They are obtained under the assumption that the orientation of the transition dipole relative to the phenyl ring is the same as in bare phenol.

According to the small angle (<20°) between the internal rotor axis and the principal c axis of the cluster, the four structures do not differ significantly. The transition dipole orientation is similar for all solutions. Due to the small differences, no distinction can be made between these four structures by comparison to the experimentally determined hybrid ratio. The angle $\angle(H_8\text{–}O_7\text{–}COM_{OH})$ can be identified in good approximation with the angle $\angle(H_8\text{–}O_7\text{–}O_M)$ (called φ in Ref. [18]) which describes the off-linearity of the hydrogen bond. A value of more than 14° for all possible structures is quite large and has to be taken as an indication of a strong dispersive interaction between the methyl group and the aromatic ring. This dispersive interaction causes the oxygen atom of methanol to be shifted off the phenol plane, an effect which is in

Table 3
The four possible structures for phenol$(CH_3OH)_1$ in the S_0 state, referring to the different combinations of signs of λ_g[a]

	1_0	2_0	3_0	4_0
Signs $(\lambda_a, \lambda_b, \lambda_c)$	$\mp,\mp,\pm$	$\pm,\mp,\pm$	$\mp,\pm,\pm$	$\pm,\pm,\pm$
$d(O_7\text{–}COM_{OH})$ (Å)	2.909	3.095	3.119	3.293
$\angle(H_8\text{–}O_7\text{–}COM_{OH})$ (°)	14.0	14.6	14.4	14.1
$\angle(COM_{OH}\text{–}O_7\text{–}C_1\text{–}C_2)$ (°)	14.8	15.2	14.3	14.7
$\angle(O_7\text{–}COM_{OH}\text{–}COM_{CH_3})$ (°)	103.7	88.2	86.3	72.6
$\angle(COM_{CH_3}\text{–}COM_{OH}\text{–}O_7\text{–}C_1)$ (°)	76.2	66.2	100.2	89.6
$\angle(\text{TDM}, a)$ (°)	58.9	58.9	59.0	58.7
$\angle(\text{TDM}, b)$ (°)	35.9	35.7	33.6	33.8
$\angle(\text{TDM}, c)$ (°)	73.9	74.2	78.2	78.5
a-type character (%)	26.7	26.7	26.4	26.9
b-type character (%)	65.6	65.9	69.4	69.1
c-type character (%)	7.7	7.4	4.2	4.0

[a] The definition of the distances, angles and dihedral angles and the numbering of the atoms is given in Fig. 3. The angles between transition dipole moment and principal axes of the cluster are given under the assumption that the direction of the transition dipole moment in phenol does not change considerably upon complexation.

accordance with the theoretical findings of Courty et al. [18]. The most distinct differences between structures 1_0–4_0 are the lengths of the hydrogen bonds. They are given in Table 3 by the distance $d(O_7\text{–}COM_{OH})$. To convert into the O–O distance $d(O_7\text{–}O_M)$, have to consider the distance of O_M and COM_{OH}. This distance is 0.057 Å, the correction to $d(O_7\text{–}COM_{OH})$ can therefore not exceed ±0.057 Å. A value of $d(O_7\text{–}O_M)$ greater than the one given for $d(O\text{–}COM_{OH})$ would mean that the methanol oxygen is farther away from the phenol than the hydrogen. This is indeed very unlikely for the proton-accepting methanol. Hence, we take the noted values of $d(O\text{–}COM_{OH})$ as upper bounds for the actual O–O distance. A comparison with the hydrogen bond length in the phenol(water) cluster ($d(O\text{–}O) = 2.93$ Å) suggests structure 1_0 to be the most probable one. Structures 2_0 and 3_0 already seem less suited with regard to the length of the hydrogen bond. In structure 2_0, the hydrogen-bond length decreases, with the distance of the methyl group to the π-system decreasing, whereas in structure 3_0, both distances decrease compared to 1_0. Structure 4_0, representing a hydrogen-bond length longer than 3.2 Å, seems extremely unlikely. Fig. 3a shows the structure of the cluster with the above-described simplification for the methanol part. This structure does not tell us anything about the orientation of the H atom of the methanol moiety nor about the configuration of the methyl group. Fig. 3b shows a plausible structure of the phenol–methanol cluster in which the H atom of methanol is oriented in a way that the free electron pair of the O atom of methanol points towards the –OH group of phenol.

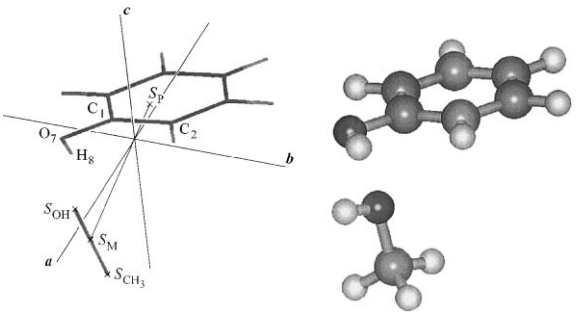

Fig. 3. (a) Definition of the structural parameters given in Table 3. The geometry shown here corresponds to structure 1_0 in the table. (b) Structure of the phenol–methanol cluster.

For the S_1 state, we repeated the above procedure with the corresponding rotational constants and internal axis angles. Furthermore, we supposed that the structural change on electronic excitation is mainly located in the aromatic chromophore. We used the phenol S_1 structure proposed by Berden et al. [6] which is deduced from the Larsen geometry [46] by increasing the C–C bond lengths and decreasing the C–O bond length. The results of our calculation are

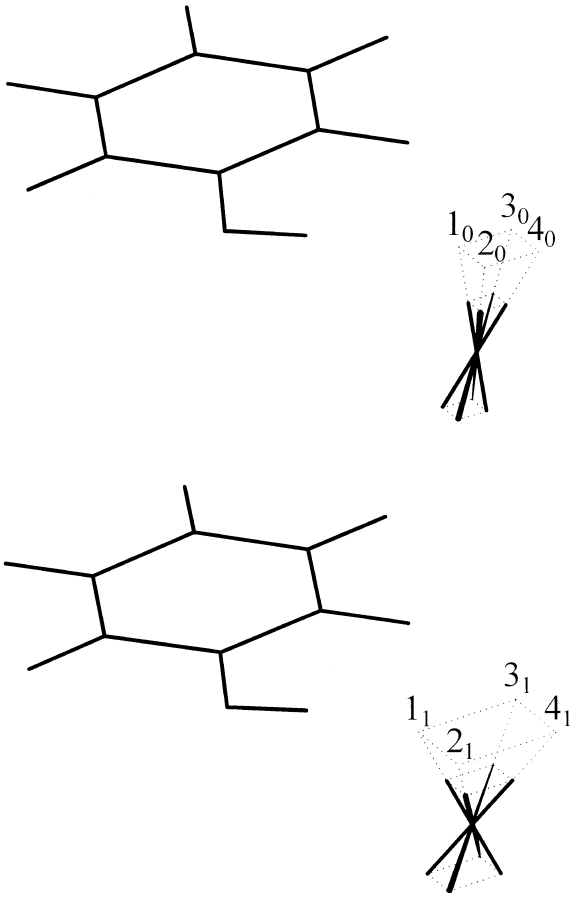

Fig. 4. (a) The four possible orientations $1_0 \ldots 4_0$ of the vector connecting the center of mass of OH and the center of mass of CH_3, relative to the phenol molecule in the S_0 state as given in Table 3. (b) The four possible orientations $1_1 \ldots 4_1$ of the vector connecting the COM of OH and the COM of CH_3 relative to the phenol molecule in the S_1 state as given in Table 4.

summarized in Table 4. The four possible structures $1_1 \ldots 4_1$ differ considerably more than the S_0 structures, owing to the increased value of $\angle(c,i)$. They are presented in Fig. 4b. The obtained distances $d(\mathrm{O–COM_{OH}})$ range between 2.8 and 3.4 Å. Again, the structure with the shortest hydrogen-bond length (1_1) seems favorable. Exclusion of the other structures is facilitated since we except $d(\mathrm{OO})[S_1] < d(\mathrm{OO})[S_0]$ due to the increased acidity of phenol in the electronically excited state. Furthermore, the polarizability of the cluster is increased in the S_1 state, leading to larger dispersion interactions between the methyl group and the aromatic π-system. This effect also leads to a general shortening of the O–O distance in the S_1 state.

5. Conclusions

The structure of the hydrogen bond in the binary phenol–methanol cluster could be determined by rotationally resolved LIF spectroscopy. We obtained four different structures, which fit equally well, the rotational constants and angles between internal rotor and inertial axes of the cluster. Three of these geometries seem more unlikely due to their large hydrogen bond distances, but cannot be ruled out completely. For the remaining structure, the O–O distance could be determined to be 2.91 ± 0.06 Å in the ground state and 2.78 ± 0.06 Å in the electronically excited state. The O–O distance in the electronic ground state of phenol–methanol is shorter than in the phenol–water cluster, which might be due to the additional dispersion forces between the methyl group and the aromatic π-system and to larger basicity of methanol compared to water. The decrease of the hydrogen-bond length upon electronic excitation is larger than in phenol–water, which can be

Table 4
Four possible structures for phenol$(CH_3OH)_1$ in the S_1 state, referring to the different combinations of signs of λ_g[a]

	1_1	2_1	3_1	4_1
Signs $(\lambda_a, \lambda_b, \lambda_c)$	$\mp,\mp,\pm$	$\pm,\mp,\pm$	$\mp,\pm,\pm$	$\pm,\pm,\pm$
$d(\mathrm{O_7–COM_{OH}})$ (Å)	2.777	3.082	3.146	3.419
$\angle(\mathrm{H_8–O_7–COM_{OH}})$ (°)	14.6	16.6	12.5	12.5
$\angle(\mathrm{COM_{OH}–O_7–C_1–C_2})$ (°)	121.4	130.3	76.3	93.3
$\angle(\mathrm{O_7–COM_{OH}–COM_{CH_3}})$ (°)	114.6	88.1	83.0	61.3
$\angle(\mathrm{COM_{CH_3}–COM_{OH}–O_7–H_8})$ (°)	−128.7	−107.1	138.3	170.4

[a] The definition of the distances, angles and dihedral angles and the numbering of the atoms is given in Fig. 3.

explained both by the increased acidity of phenol as well as by the increased polarizability of the cluster the S_1 state. The internal rotor axis of the methanol unit, which nearly coincides with the C–O axis is almost perpendicular to the aromatic plane. This means a distinct deviation from the translinear hydrogen-bond geometry which was found in the phenol–water complex. The interaction between the methyl group and the π-system of phenol bends the hydrogen bond from linearity to an angle of 14° both in the S_0 and S_1 states. The reduced stability of the nonlinear hydrogen bond can be compensated by the dispersive interaction of the methyl group with the aromatic π-system.

The barrier to internal rotation of the methyl group decreases upon electronic excitation from 170 cm^{-1} in the ground state to 146 cm^{-1} in the excited state. The reduction of the barrier height could be explained by the increased acidity of phenol upon electronic excitation, whereas the small absolute value compared to the barrier in free methanol appears to be an artifact due to the one-dimensional description of the large amplitude motion.

Acknowledgements

We would like to thank Professor Kleinermanns for his continuous support, for his steady interest in this work and for many helpful discussions. The help of Professor Wolfgang Stahl, who put the microwave rotational constants of phenol–methanol at our disposal prior to publication is gratefully acknowledged. We thank the Deutsche Forschungsgemeinschaft for financial support of this work. This work is part of the Dissertation of Arnim Westphal.

References

[1] H. Abe, N. Mikami, M. Ito, J. Phys. Chem. 86 (1982) 1768.
[2] A. Sur, P.M. Johnson, J. Chem. Phys. 84 (1986) 1206.
[3] R.J. Stanley, A.W. Castleman Jr., J. Chem. Phys. 94 (1991) 7744.
[4] R.J. Lipert, S.D. Colson, J. Chem. Phys. 89 (1988) 4579.
[5] M. Schütz, T. Bürgi, S. Leutwyler, T. Fischer, J. Chem. Phys. 98 (1993) 3763.
[6] G. Berden, W. Meerts, M. Schmitt, K. Kleinermanns, J. Chem. Phys. 104 (1996) 972.
[7] M. Gerhards, M. Schmitt, K. Kleinermanns, W. Stahl, J. Chem. Phys. 104 (1996) 967.
[8] M. Schmitt, C. Jacoby, K. Kleinermanns, J. Chem. Phys. 108 (1998) 4486.
[9] R.M. Helm, H.-P. Vogel, H.J. Neusser, J. Chem. Phys. 108 (1998) 4496.
[10] T. Ebata, M. Furukawa, T. Suzuki, M. Ito, J. Opt. Soc. Am. B 7 (1990) 1890.
[11] O. Dopfer, K. Müller-Dethlefs, J. Chem. Phys. 101 (1994) 8508.
[12] T. Watanabe, T. Ebata, S. Tanabe, N. Mikami, J. Chem. Phys. 105 (1996) 408.
[13] S. Tanabe, T. Ebata, M. Fujii, N. Mikami, Chem. Phys. Lett. 215 (1993) 347.
[14] H. Abe, N. Mikami, M. Ito, Y. Udagawa, J. Phys. Chem. 86 (1982) 2567.
[15] T.G. Wright, E. Cordes, O. Dopfer, K. Müller-Dethlefs, J. Chem. Soc. Faraday Trans. 89 (1993) 1601.
[16] M. Gerhards, K. Beckmann, K. Kleinermanns, Z. Phys. D 29 (1994) 223.
[17] M. Schmitt, H. Müller, U. Henrichs, M. Gerhards, W. Perl, C. Deusen, K. Kleinermanns, J. Chem. Phys. 103 (1995) 584.
[18] A. Courty, M. Mons, B. Dimicoli, F. Piuzzi, V. Brenner, P. Millié, J. Phys. Chem. A 102 (1998) 4890.
[19] R.J. Lipert, S.D. Colson, J. Phys. Chem. 93 (1989) 3894.
[20] E. Cordes, O. Dopfer, T.G. Wright, K. Müller-Dethlefs, J. Phys. Chem. 97 (1993) 7471.
[21] J.A. Syage, in: J. Manz, L. Wöste (Eds.), Femtosecond Chemistry, Verlag Chemie, 1995.
[22] M.F. Hineman, D.F. Kelley, E.R. Bernstein, J. Chem. Phys. 99 (1993) 4533.
[23] N. Mikami, A. Okabe, I. Suzuki, J. Phys. Chem. 92 (1988) 1858.
[24] A. Schiefke, C. Deusen, C. Jacoby, M. Gerhards, M. Schmitt, K. Kleinermanns, P. Hering, J. Chem. Phys. 102 (1995) 9197.
[25] A. Crepin, A. Tramer, Chem. Phys. 156 (1991) 281.
[26] D. Solgadi, C. Jouvet, A. Tramer, J. Phys. Chem. 92 (1988) 3313.
[27] W. Siebrand, M.Z. Zgierski, Z.K. Smedarchina, M. Vener, J. Kaneti, Chem. Phys. Lett. 266 (1997) 47.
[28] N. Gonohe, H. Abe, N. Mikami, M. Ito, J. Phys. Chem. 89 (1985) 3642.
[29] G. Hartland, B. Henson, V. Venturo, P.M. Felker, J. Phys. Chem. 96 (1992) 1164.
[30] W. Stahl, private communication.
[31] U. Gudladt, Mikrowellenspektroskopische Untersuchungen des Komplexes Phenol–Methanol, Diplomarbeit, Christian Albrechts Universität, Kiel, 1996.
[32] J. Kraitchman, Amer. J. Phys. 21 (1953) 17.
[33] M. Schmitt, Spektroskopische Untersuchungen an Wasserstoffbrückenbindungen, Habilitation, Heinrich-Heine-Universität, Düsseldorf, 2000.
[34] T.W. Hänsch, B. Couillaud, Opt. Commun. 35 (1980) 441.

[35] S. Gerstenkorn, P. Luc, Atlas du spectre d'absorption de la molecule d'iode 14800–20000 cm^{-1}, CNRS, Paris, 1986.
[36] P.R. Bunker, P. Jensen, Molecular Symmetry and Spectroscopy, 2nd ed., NRC Research Press, Ottawa, Ont., Canada, 1998.
[37] W. Gordy, R.L. Cook, Microwave Molecular Spectra, third ed., Wiley, New York, 1984.
[38] C.C. Lin, J.D. Swalen, Rev. Mod. Phys. 31 (1959) 841.
[39] J.K.G. Watson, J. Chem. Phys. 46 (1967) 1935.
[40] J.K.G. Watson, J. Chem. Phys. 48 (1968) 4517.
[41] D.R. Herschbach, J. Chem. Phys. 31 (1959) 91.
[42] D.F. Plusquellic, D.W. Pratt, J. Chem. Phys. 97 (1992) 8970.
[43] M.C.L. Gerry, R.M. Lees, G. Winnewisser, J. Mol. Spec. 61 (1976) 231.
[44] F.J. Lovas, S.P. Belov, M.Y. Tretyakov, W. Stahl, R.D. Suenram, J. Mol. Spec. 170 (1995) 478.
[45] G.T. Fraser, F.J. Lovas, R.D. Suenram, J. Mol. Spec. 167 (1994) 231.
[46] N.W. Larsen, J. Mol. Struct. 51 (1979) 175.
[47] R.N. Zare, Angular Momentum, Wiley, New York, 1988.
[48] J.K.G. Watson, J. Mol. Spec. 66 (1977) 500.